Supporting Information

Building dual-phased Ni_2P-$Ni_2P_4O_{12}$ electrocatalysts for efficient urea oxidation reaction

Jiajia Zhou,[a] Xiujuan Sun,[a] Wenjuan Tan,[a] Qiuhan Cao,[a] Yongjie Zhao,[a] Rui Ding,[a] Yuwei Zhang,*[b] Enhui Liu[a] and Ping Gao[a]*

[a]Key Laboratory of Environmentally Friendly Chemistry and Applications of Ministry of Education, College of Chemistry, Xiangtan University, Hunan 411105, P.R. China.

[b]Guangzhou Key Laboratory of Sensing Materials & Devices,School of Chemistry and Chemical Engineering, Guangzhou University, Guangzhou 510006, P.R. China.

*Corresponding authors E-mail: sunxj594@xtu.edu.cn; ccywzhang@gzhu.edu.cn

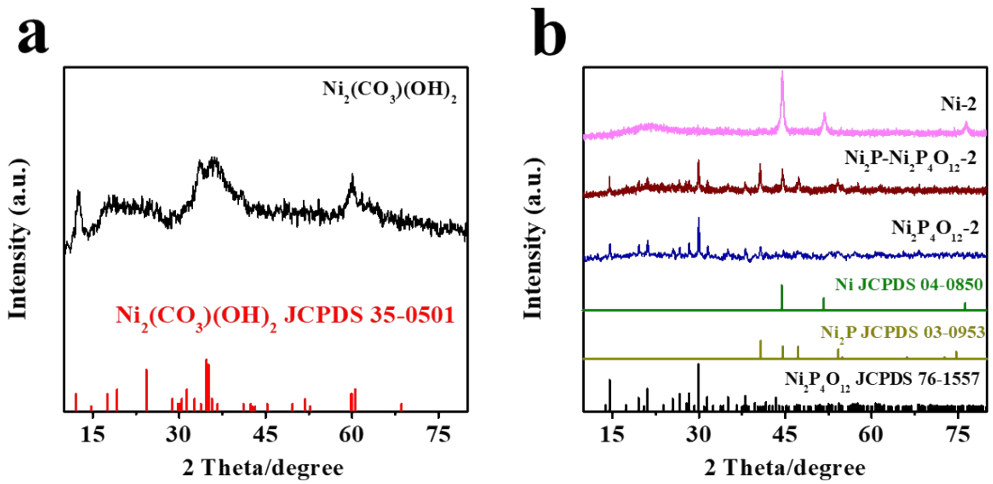

Fig. S1 XRD patterns of (a) the precursor; (b) Ni-2, Ni_2P-$Ni_2P_4O_{12}$-2, $Ni_2P_4O_{12}$-2

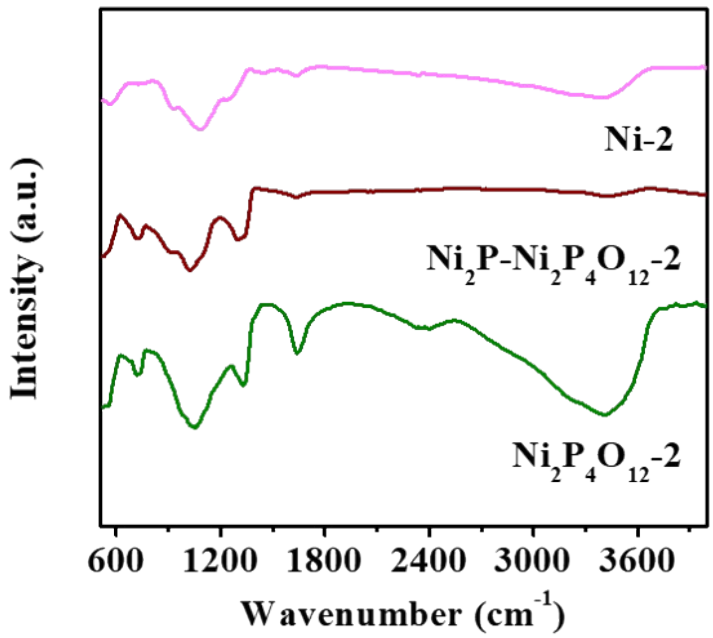

Fig. S2 The FT-IR of Ni-2, Ni_2P-$Ni_2P_4O_{12}$-2, $Ni_2P_4O_{12}$-2.

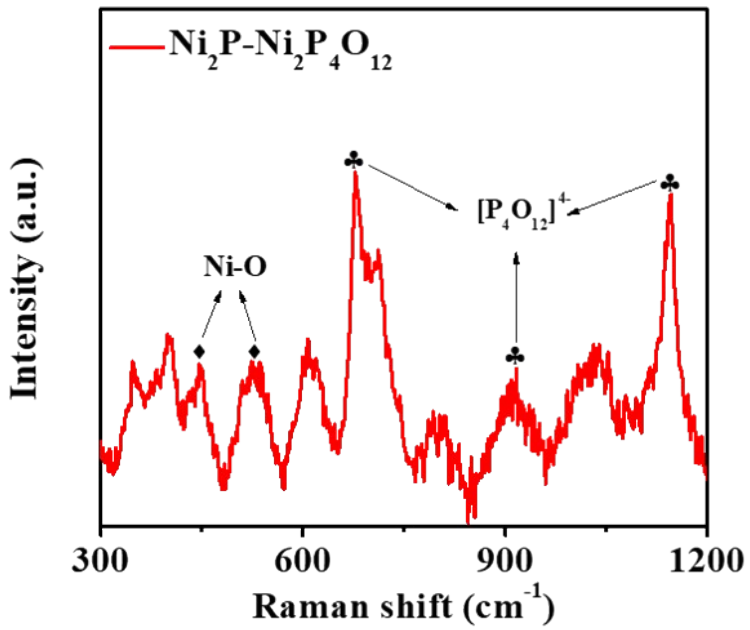

Fig. S3 The Raman spectra of Ni_2P-$Ni_2P_4O_{12}$.

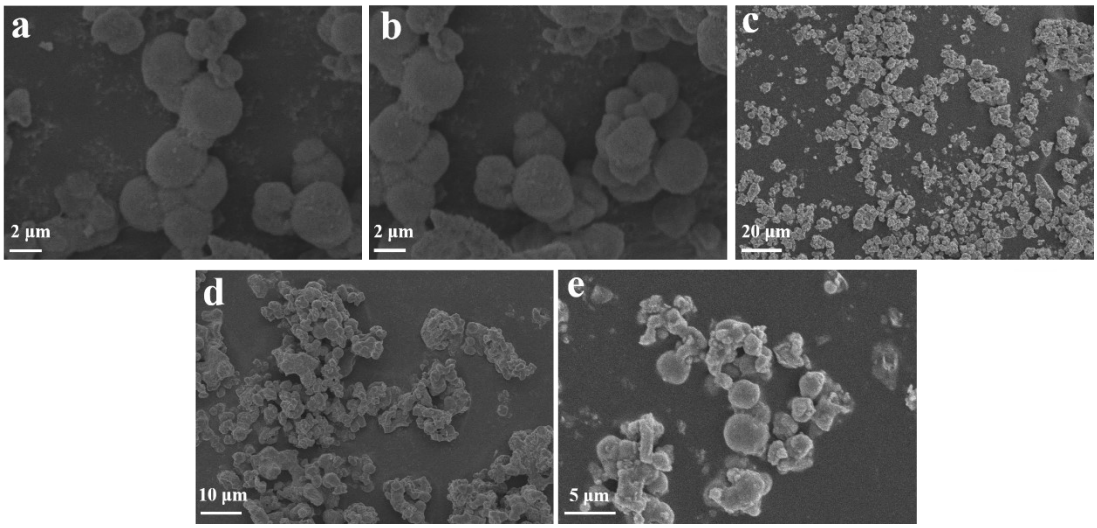

Fig. S4 The SEM images of (a) Ni, (b) Ni-2, (c) Ni_2P-$Ni_2P_4O_{12}$-2, (d) $Ni_2P_4O_{12}$, and (e) $Ni_2P_4O_{12}$-2.

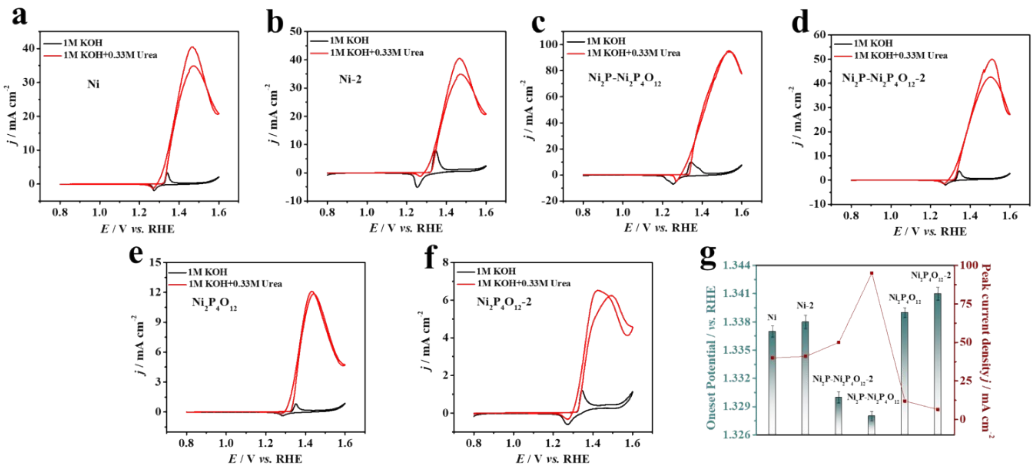

Fig. S5 The CV curves (10 mV s^{-1}) of (a) Ni, (b) Ni-2, (c) Ni_2P-$Ni_2P_4O_{12}$-2, (d) Ni_2P-$Ni_2P_4O_{12}$, (e) $Ni_2P_4O_{12}$, (f) $Ni_2P_4O_{12}$-2 in 1 M KOH solution with the presence/absence of 0.33 M urea and (g) onset-potentials (E_{onset}) and peak current densities (J_p) of different samples.

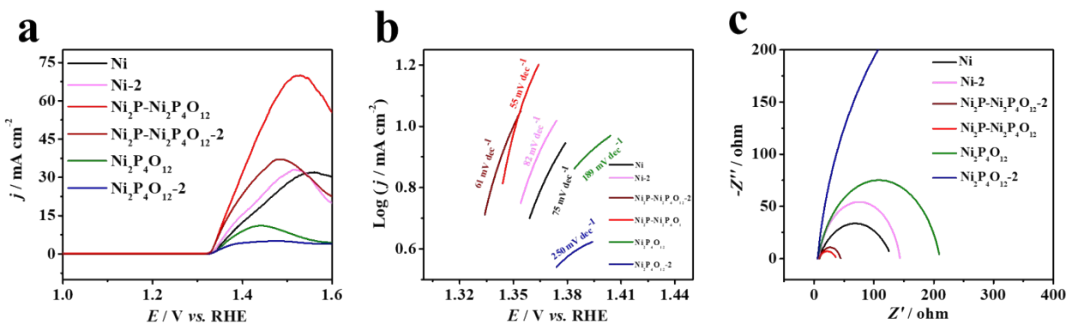

Fig. S6 The UOR performance of different catalysts. (a) Polarization curves of various catalysts at 5 mV s^{-1} in 1 M KOH + 0.33 M urea. (b) The Tafel slopes. (c) Nyquist plots at 1.35 V *vs.* RHE.

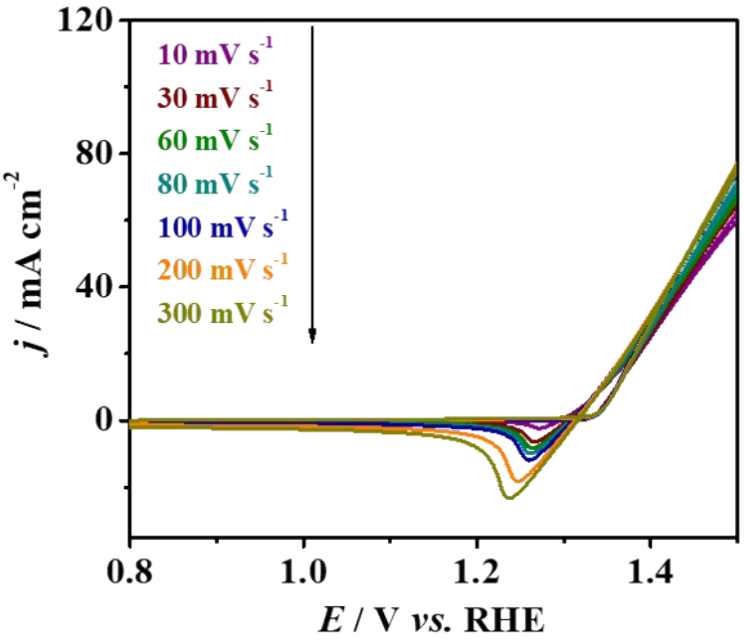

Fig. S7 UOR polarization plots of Ni_2P-$Ni_2P_4O_{12}$ catalyst at different scan rates.

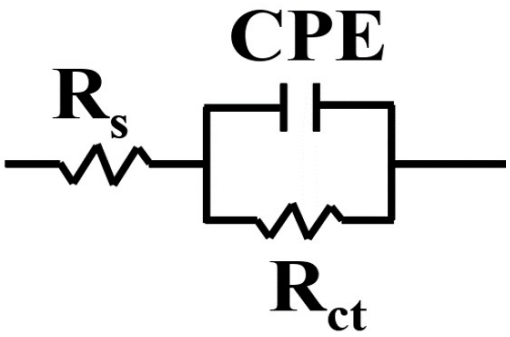

Fig. S8 The Nyquist Plots of as prepared samples are fitted to a simplified equivalent model.

The equivalent circuit model consisting of three parts: R_{ct} is the charge transfer resistance, R_s is donated as the bulk solution resistance and CPE corresponds the constant phase element.

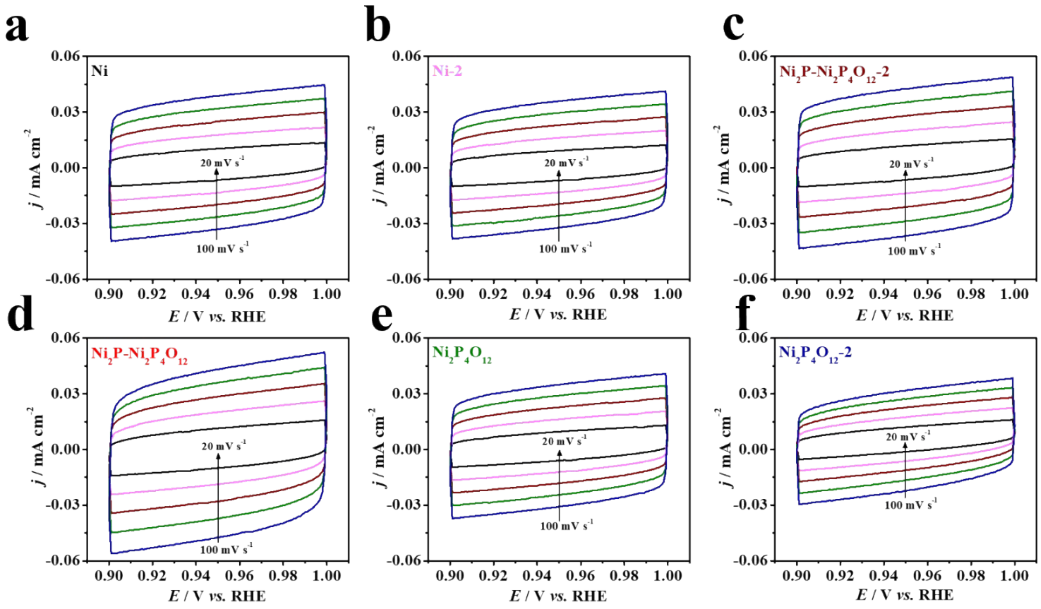

Fig. S9 Cyclic voltammograms (CV) of (a) Ni, (b) Ni-2, (c) Ni_2P-$Ni_2P_4O_{12}$-2, (d) Ni_2P-$Ni_2P_4O_{12}$, (e) $Ni_2P_4O_{12}$ and (f) $Ni_2P_4O_{12}$-2 at different scan rates of 20, 40, 60, 80, and 100 mV s^{-1} in 1 M KOH solution for C_{dl} testing at non-faradic reaction potential region for UOR.

The electrochemical active surface area (ECSA) was estimated in 1.0 M KOH in terms of the double-layer capacitances (C_{dl}) from cyclic voltammetry (CV) at the scan rates of 20-100 mV s^{-1} (20, 40, 60, 80, 100 mV s^{-1}). The potential range of the measurements is from 0.9 to 1 V *vs.* RHE in a non-Faradaic region. The current density differences ($\Delta j = j_a - j_c$) at 0.95 V *vs.* RHE were plotted against scan rates, and the linear slope is the C_{dl}.

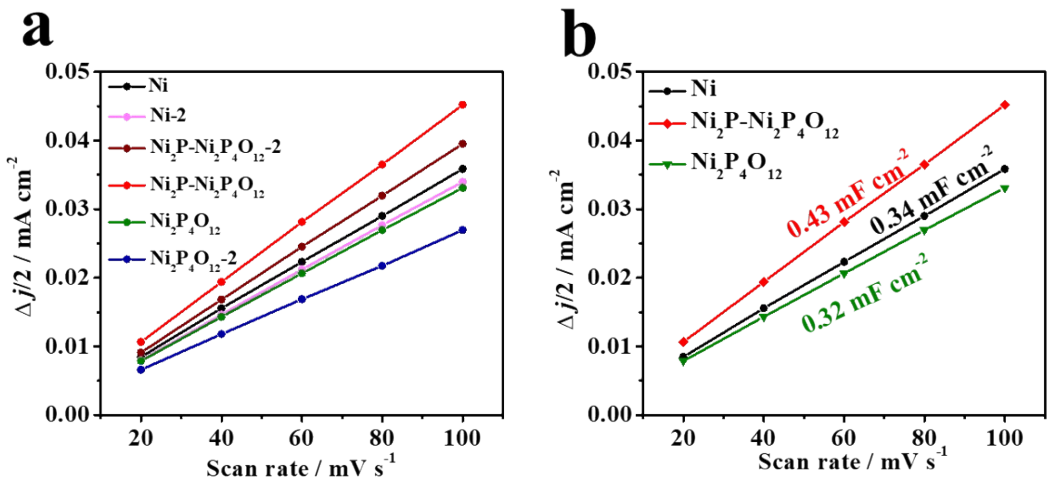

Fig. S10 The charging current density differences plotted against scan rates of the as-prepared catalysts. The linear slope is equivalent to electrochemical double-layer capacitance (C_{dl}).

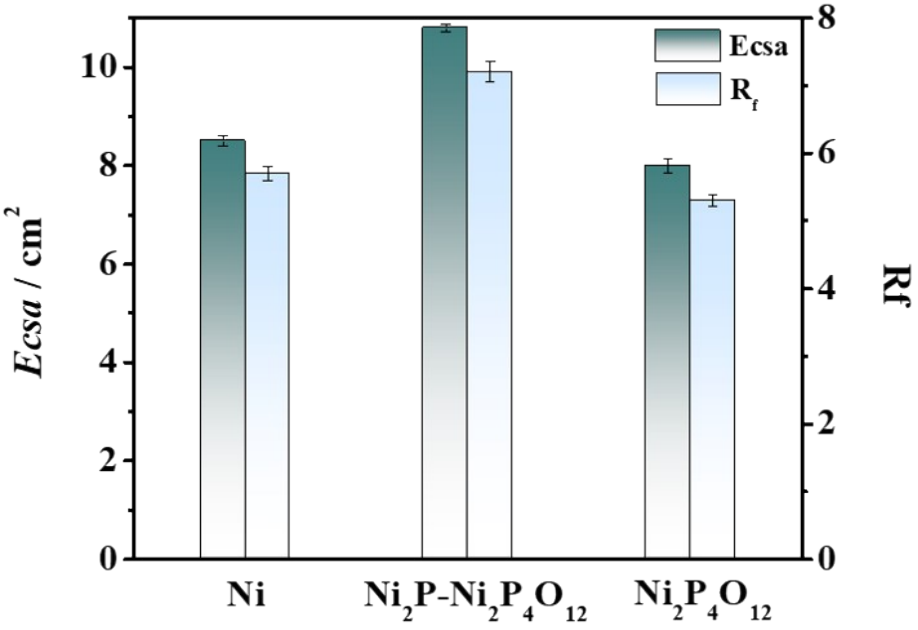

Fig. S11 Electrochemical active surface area (ECSA) and roughness factors (R_f) of different samples.

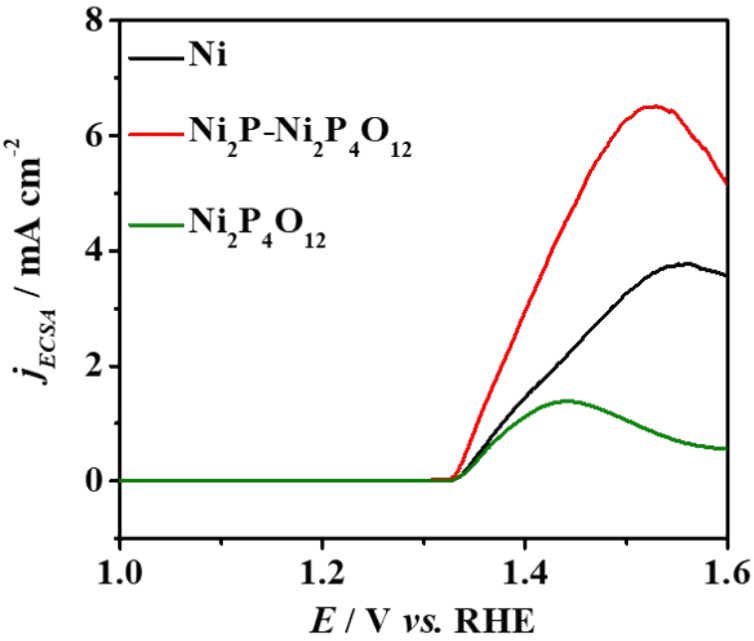

Fig. S12 ESCA-normalized LSV curves of Ni, Ni_2P-$Ni_2P_4O_{12}$ and $Ni_2P_4O_{12}$.

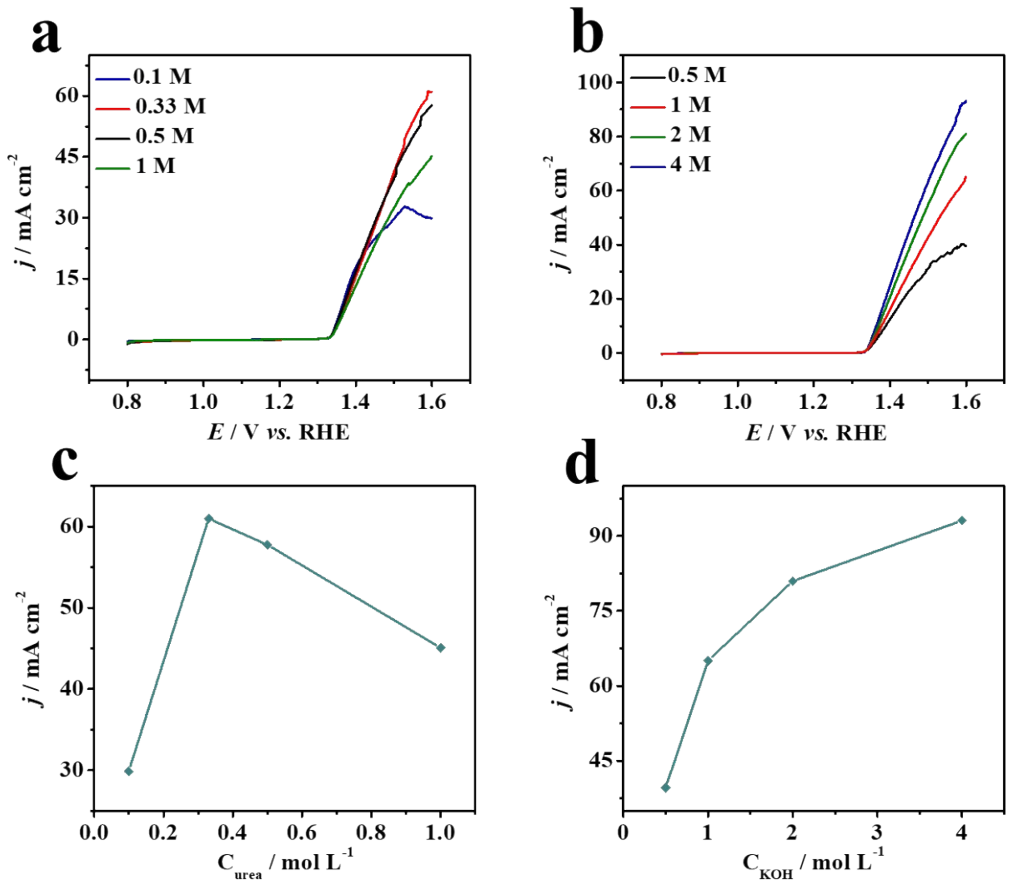

Fig. S13 The UOR performance of Ni_2P-$Ni_2P_4O_{12}$ catalyst (a), (c) in 1.0 M KOH with various urea concentrations, (b), (d) in 0.33 M urea with various KOH concentrations.

The influence of urea concentrations was tested in 1 M KOH solution on Ni_2P-$Ni_2P_4O_{12}$ electrode at a scan rate of 5 mV s^{-1} and shown in Fig. S13a, c. The oxidation current density y increases linearly from 0.1 M to 0.33 M urea, subsequently decreases at concentrations of urea higher than 0.33 M, which can be attributed to the fact that the NiOOH active sites are occupied by excessive urea molecules, resulting in local OH^- species deprivation and thus reduced UOR performance. Also, the effect of KOH concentration in 0.33 M urea is shown in Fig. S13b, d. It can clearly see that the current density with increasing OH^- concentration, while the onset potential decreases with the raise of KOH concentration. This can be interpreted as a higher OH concentration favoring the generation of NiOOH active sites.

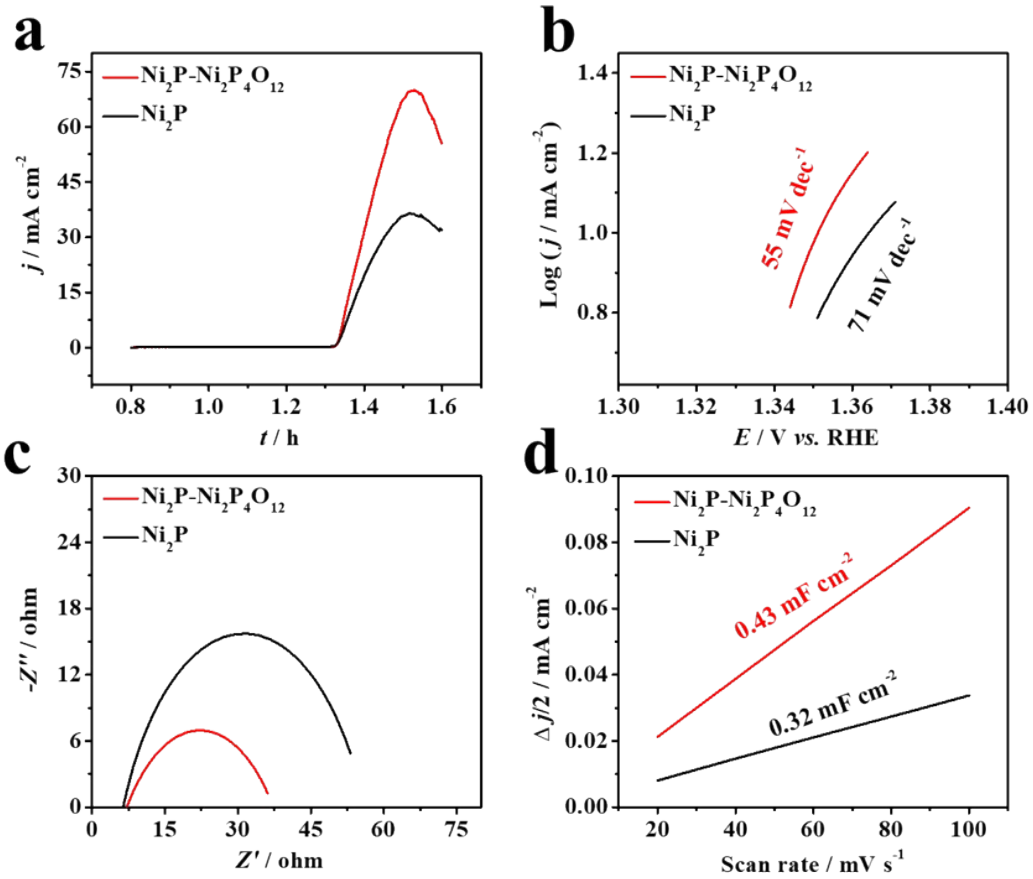

Fig. S14. The electrochemical properties of Ni_2P-$Ni_2P_4O_{12}$ and Ni_2P, respectively.

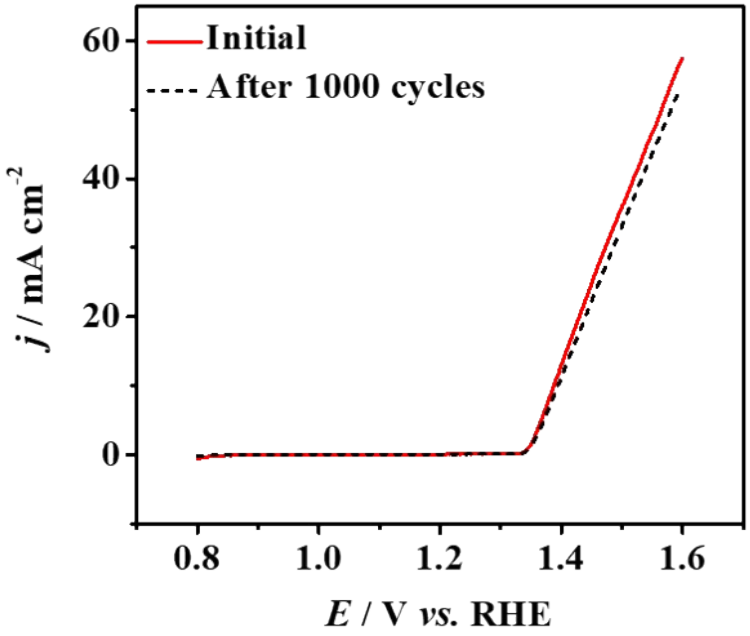

Fig. S15 The polarization curve before and after 1000 CV cycles of Ni_2P-$Ni_2P_4O_{12}$ (The catalyst was loaded on the carbon cloth).

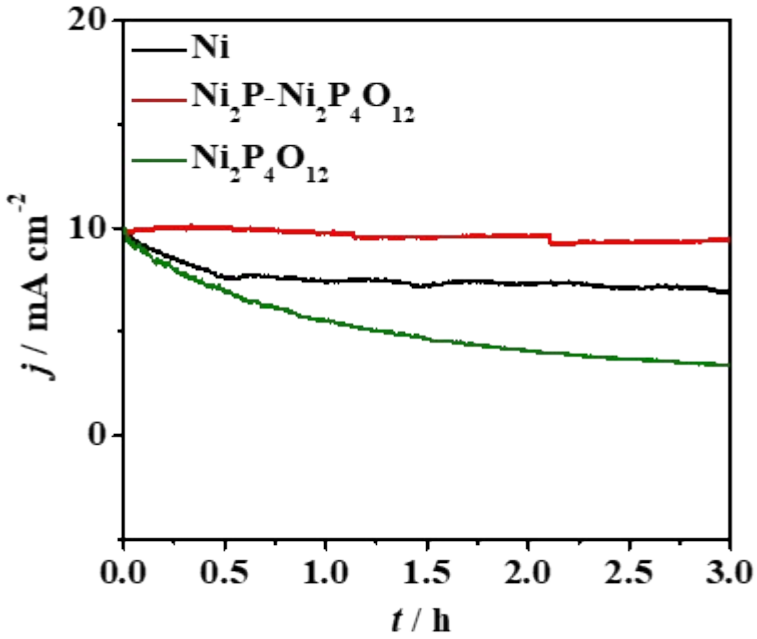

Fig. S16 The chronoamperometric stability for 3 h for Ni, Ni_2P-$Ni_2P_4O_{12}$ and $Ni_2P_4O_{12}$.

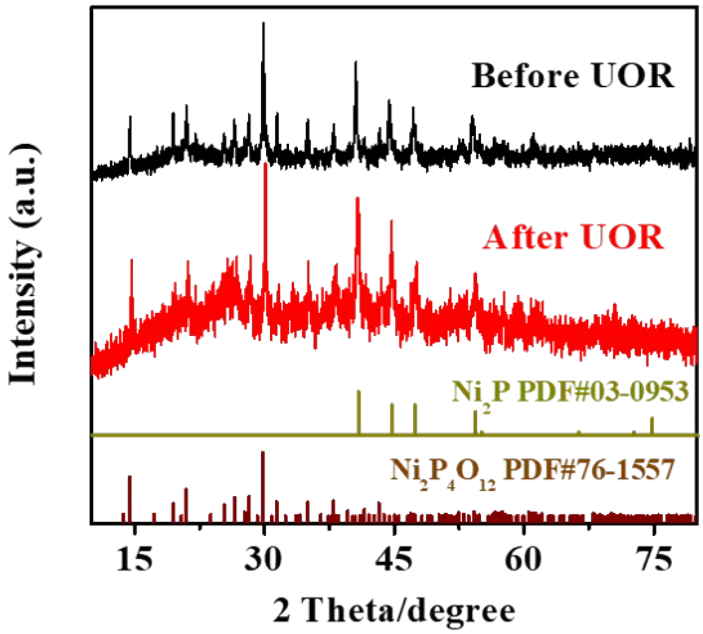

Fig. S17 The XRD patterns of Ni_2P-$Ni_2P_4O_{12}$ before and after stability test.

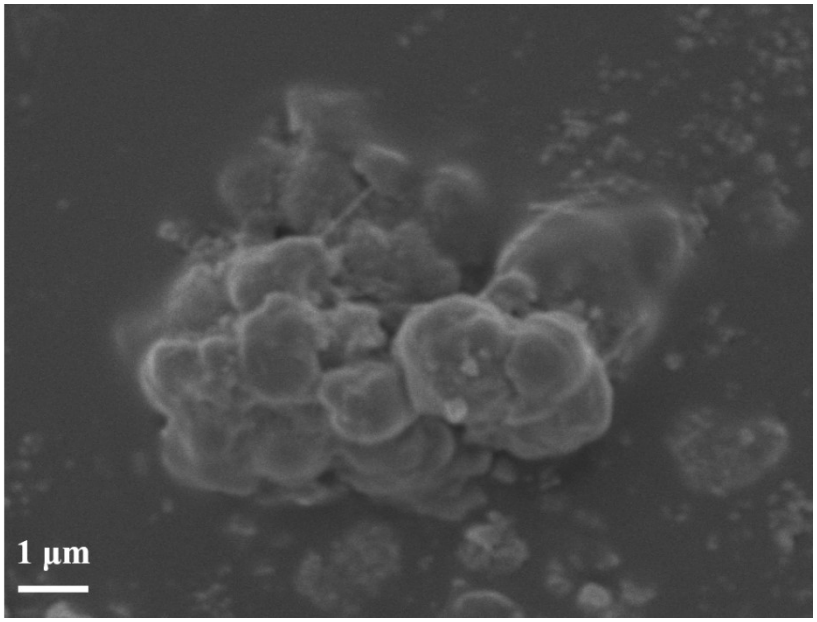

Fig. S18 The SEM image of Ni_2P-$Ni_2P_4O_{12}$ after stability test.

Table S1. The formation mechanism of the three catalysts can be understood by following reaction processes

	Reaction mechanism
(1)	$2H_2PO_2^- \rightarrow PH_3\uparrow + HPO_4^{2-}$
(2)	$16Ni^{2+} + 9PH_3 + 4H_2O \rightarrow 8Ni_2P + HPO_4^{2-} + 34H^+$
(3)	$HPO_4^{2-} \rightarrow PO_3^- + OH^-$
(4)	$4Ni^{2+} + PH_3 + 4H_2O \rightarrow 4Ni + HPO_4^{2-} + 10H^+$
(5)	$Ni^{2+} + 2PO_3^- \rightarrow Ni_2P_4O_{12}$ ↘ ↑ **aggregation** $Ni(PO_3)_2$

Table S2. Ni and P content determined by ICP results of Ni_2P-$Ni_2P_4O_{12}$ (The sample was averaged over three tests).

Sample	Ni (mg/mL)	P (mg/mL)
Ni_2P-$Ni_2P_4O_{12}$	337.8 ± 0.85	214.9 ± 0.73

Table S3. The XPS binding energies of Ni 2p, P 2p, and O 1s for Ni, Ni_2P-$Ni_2P_4O_{12}$, $Ni_2P_4O_{12}$, respectively.

Sample	Ni 2p	P 2p	O 1s
Ni	852.73 eV, 869.07 eV (Ni^0) 856.22 eV, 873.99 eV (Ni^{2+}) 861.29 eV, 879.75 eV (Sat.)	/	/
Ni_2P-$Ni_2P_4O_{12}$	**852.97 eV (Ni^0)** **856.69 eV, 874.52 eV (Ni^{2+})** **861.77 eV, 880.42 eV (Sat.)** **858.32 eV, 876.67 eV (Ni^{3+})**	**133.66 eV (P-O-Ni species)** **134.44 eV (PO_3^-)**	**531.44 eV (P-O-Ni species)** 533.11 eV (**PO_3^-**)
$Ni_2P_4O_{12}$	856.14 eV, 873.46 eV (Ni^{2+}) 861.72 eV, 879.78 eV (Sat.) 858.3 eV, 874.96 eV (Ni^{3+})	133.79 eV (P-O-Ni species) 134.39 (PO_3^-)	531.83 eV (P-O-Ni species) 533.28 eV (PO_3^-)

Table S4. Comparison of UOR performance for Ni_2P-$Ni_2P_4O_{12}$ and recent reported electrocatalyst tested on glass carbon electrode (GCE).

Catalysts	Electrolyte	Potential at 10 mA cm^{-2} (V)	Tafel Slope (mV dec^{-1})	Ref.
Ni_2P-$Ni_2P_4O_{12}$	**1.0 M KOH+ 0.33 M urea**	**1.35**	**55**	**This work**
NiOH-D	1.0 M KOH+ 0.33 M urea	1.38	74	[1]
Metallic $Ni(OH)_2$	1.0 M KOH+ 0.33 M urea	1.38	/	[2]
NiS_2-MoS_2	1.0 M KOH+ 0.33 M urea	1.52	62.3	[3]
NiCr/C	1.0 M KOH+ 0.33 M urea	1.38	/	[4]
Ni/Sn dendrites	1.0 M KOH+ 0.33 M urea	1.41	35	[5]
Pristine Ni MOF	1.0 M KOH+ 1 M urea	1.36	64	[6]
Ni_2P	1.0 M KOH+ 0.5 M urea	1.35	100	[7]
NiMn/C	1.0 M KOH+ 0.33 M urea	1.40	/	[8]
Ni/C-1	1.0 M KOH+ 0.33 M urea	1.39	62	[9]

[1] L.S. Zhang, L.P. Wang, H.P. Lin, Y.X. Liu, J.Y. Ye, Y.Z. Wen, A. Chen, L. Wang, F.L. Ni, Z.Y. Zhou, S.G. Sun, Y.Y. Li, B. Zhang, H.S. Peng, A Lattice-Oxygen-Involved Reaction Pathway to Boost Urea Oxidation, Angew. Chem., Int. Ed., 58 (2019) 16820-16825.

[2] X.J. Zhu, X.Y. Dou, J. Dai, X.D. An, Y.Q. Guo, L.D. Zhang, S. Tao, J.Y. Zhao, W.S. Chu, X.C. Zeng, C.Z. Wu, Y. Xie, Metallic Nickel Hydroxide Nanosheets Give Superior Electrocatalytic Oxidation of Urea for Fuel Cells, Angew. Chem., Int. Ed., 55 (2016) 12465-12469.

[3] S.L. Wang, L.Y. Zhao, J.X. Li, X.L. Tian, X. Wu, L.G. Feng, High valence state of Ni and Mo synergism in NiS_2-MoS_2 hetero-nanorods catalyst with layered surface structure for urea electrocatalysis, J. Energy Chem., 66 (2022) 483-492.

[4] R.K. Singh, A. Schechter, Electroactivity of NiCr Catalysts for Urea Oxidation in Alkaline Electrolyte, Chemcatchem, 9 (2017) 3374-3379.

[5] R.K. Singh, P. Subramanian, A. Schechter, Enhanced Urea Activity of Oxidation on Nickel-Deposited Tin Dendrites, Chemelectrochem, 4 (2017) 1037-1043.

[6] V. Maruthapandian, S. Kumaraguru, S. Mohan, V. Saraswathy, S. Muralidharan, An Insight on the Electrocatalytic Mechanistic Study of Pristine Ni MOF (BTC) in Alkaline Medium for Enhanced OER and UOR, Chemelectrochem, 5 (2018) 2795-2807.

[7] H.P. Liu, S.L. Zhu, Z.D. Cui, Z.Y. Li, S.L. Wu, Y.Q. Liang, Ni_2P nanoflakes for the high-performing urea oxidation reaction: linking active sites to a UOR mechanism, Nanoscale, 13 (2021) 1759-1769.

[8] N.A.M. Barakat, M. Alajami, Y. Al Haj, M. Obaid, S. Al-Meer, Enhanced onset potential NiMn-decorated activated carbon as effective and applicable anode in urea fuel cells, Catal. Commun., 97 (2017) 32-36.

[9] L. Wang, L.T. Ren, X.R. Wang, X. Feng, J.W. Zhou, B. Wang, Multivariate MOF-Templated Pomegranate-Like Ni/C as Efficient Bifunctional Electrocatalyst for Hydrogen Evolution and Urea Oxidation, ACS Appl. Mater. Interfaces, 10 (2018) 4750-4756.

Table S5 EIS fitting parameters from equivalent circuits for all samples.

Samples	R_s	R_{ct}	CPE
Ni	7.20	117.90	3.15×10^{-3}
Ni-2	7.86	127.74	2.12×10^{-3}
Ni_2P-$Ni_2P_4O_{12}$	**7.14**	**23.03**	**8.25×10^{-3}**
Ni_2P-$Ni_2P_4O_{12}$-2	9.18	26.03	1.83×10^{-3}
$Ni_2P_4O_{12}$	6.32	197.88	8.17×10^{-4}
$Ni_2P_4O_{12}$-2	5.98	732.02	2.25×10^{-8}